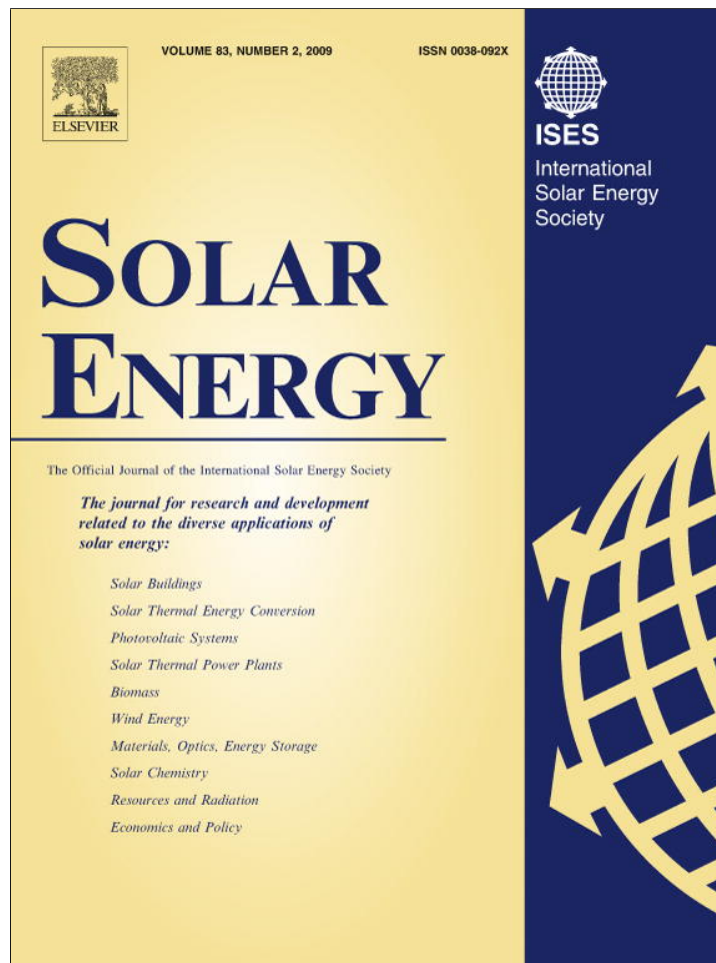


Provided for non-commercial research and education use.
Not for reproduction, distribution or commercial use.



This article appeared in a journal published by Elsevier. The attached copy is furnished to the author for internal non-commercial research and education use, including for instruction at the authors institution and sharing with colleagues.

Other uses, including reproduction and distribution, or selling or licensing copies, or posting to personal, institutional or third party websites are prohibited.

In most cases authors are permitted to post their version of the article (e.g. in Word or Tex form) to their personal website or institutional repository. Authors requiring further information regarding Elsevier's archiving and manuscript policies are encouraged to visit:

<http://www.elsevier.com/copyright>



On the validity of a design method for a solar-assisted ejector cooling system

S. Colle^{a,*}, G.S. Pereira^{a,2}, H.R. Vidal Gutiérrez^b, R. Escobar Moragas^c

^a LABSOLAR (Solar Energy Laboratory)/LEPTEN, Department of Mechanical Engineering, Universidade Federal de Santa Catarina, P.O. Box 88040-900, Florianópolis, SC, Brazil

^b Department of Mechanical Engineering, Universidad de Magallanes, P.O. Box 113-D, Punta Arenas, Chile

^c Department of Mechanical and Metallurgical Engineering, Pontificia Universidad Católica de Chile, Vicuña Mackenna 4860, Santiago, Chile

Received 20 December 2007; received in revised form 3 July 2008; accepted 10 July 2008

Available online 5 August 2008

Communicated by: Associate Editor Rhzhu Wang

Abstract

A solar-assisted ejector cooling system is simulated in order to investigate the validity of a design methodology. Hourly simulation results allow for computing the solar fraction, in cases when the cooling capacity of the ejector cycle is kept constant during daily periods. The computed solar fraction is compared with estimates obtained from the $f-\bar{\phi}$ -chart method based on the utilizability concept. An equivalent minimum temperature for the utilizability of the solar system is found, which proves to be different, but close to, the vapor generator temperature of the ejector cycle. It is shown that the solar fraction derived from the utilizability concept based on the monthly means of the global solar radiation is applicable to solar-assisted ejector cooling cycles, in cases when the minimum temperature at which solar heat is supplied to the load is determined. Good agreement is found between the solar fraction results obtained from the simulations and those obtained by the $f-\bar{\phi}$ -chart method.

© 2008 Elsevier Ltd. All rights reserved.

Keywords: Solar fraction; Solar cooling; Ejector; $f-\bar{\phi}$ -chart

1. Introduction

The past decades have seen an increase on research leading to develop renewable energy systems as a measure to achieve substantial reduction in emissions of greenhouse effect gases. Solar energy is considered worldwide as an effective renewable energy alternative; with potential to contribute to reductions in fossil fuel and electric energy consumption, mostly for domestic air and water heating applications. Collectors of the flat plate and evacuated tube types are cost effective for many applications in domestic

and industrial process heat, if the required temperatures are lower than 100 °C. The situation is different for solar-assisted cooling cycles, which are hardly competitive with mechanical compression cycles (Arbel and Sokolov, 2004), mostly due to the high capital cost associated with the acquisition of a large number of solar collectors needed to supply the required heat, and the relatively long payback time. Regarding solar driven absorption cooling systems, there are only a few applications in which they can be competitive with mechanical compression (Herold et al., 1996). Capital cost of solar collectors, and barriers arising from architecture constraints, contribute to reduce the economical advantages in favor of absorption cooling cycles. Furthermore, mechanical compressors have decreased their cost and have become more efficient in the past years. The situation is not better for ejector cooling cycles. The coefficient of performance (COP) of a single stage lithium

* Corresponding author. Tel.: +55 48 3234 0408; fax: +55 48 3721 7615.

E-mail addresses: colle@emc.ufsc.br (S. Colle), humberto.vidal@u-mag.cl (H.R. Vidal Gutiérrez), rescobar@ing.puc.cl (R.E. Moragas).

¹ ISES member.

² Currently with PETROBRAS.

Nomenclature

A_c	solar collector area (m^2)	T_s	temperature of the solar heating system working fluid ($^{\circ}C$)
A_{ev}	effective heat exchanger area – changing phase section (m^2)	U_{ev}	global heat transfer coefficient for the changing phase section of the heat exchanger ($kW/m^2^{\circ}C$)
A_s	effective heat exchanger area – single-phase section (m^2)	U_L	solar collector heat loss coefficient ($kW/m^2^{\circ}C$)
A_{rcs}	total heat exchanger area (m^2)	U_s	global heat transfer coefficient for the single-phase section of the heat exchanger ($kW/m^2^{\circ}C$)
c_p	specific heat of the solar heating system working fluid ($kJ/kg^{\circ}C$)	W_{max}	maximum hourly thermal capacitance between $(\omega c_p)_s$ and $\omega_{ej}c_{rl}$ ($kW/^{\circ}C$)
c_{rl}	specific heat of the ejector working fluid – saturated liquid ($kJ/kg^{\circ}C$)	W_{min}	minimum hourly thermal capacitance between $(\omega c_p)_s$ and $\omega_{ej}c_{rl}$ ($kW/^{\circ}C$)
COP	coefficient of performance of the ejector cycle	x_f	vapor quality
f	hourly solar fraction	<i>Greeks</i>	
f_a	annual solar fraction	ε	heat exchanger effectiveness
f_{ϕ}	annual solar fraction given by the $f-\bar{\phi}$ -chart correlation	$\bar{\phi}$	monthly utilizability of the solar collector
F_R	heat removal factor of the solar collector	ω	mass flow rate of working fluid (kg/s)
h_c	enthalpy of the ejector working fluid at temperature	$(\omega c_p)_s$	hourly thermal capacitance of the solar heating working fluid ($kW/^{\circ}C$)
T_c	subcooled state (kJ/kg)	$\omega_{ej}c_{rl}$	hourly thermal capacitance of the ejector working fluid ($kW/^{\circ}C$)
h_l	enthalpy of the saturated liquid (kJ/kg)	$(\tau\alpha)$	normal transmittance – absorptance factor of the solar collector
h_v	enthalpy of the saturated vapor (kJ/kg)	<i>Subscripts and Superscripts</i>	
$K_{\tau\alpha}$	incidence angle modifier	s	single phase (heat exchanger effectiveness)
Q_{aux}	auxiliary heat power (kW)	ej	ejector working fluid mass rate
Q_g	heat power input to the vapor generator of the ejector cycle (kW)	ev	two-phase (heat exchanger effectiveness)
Q_r	ejector cycle cooling load (kW)	n	normal
T_c	temperature of the ejector subcooled working fluid ($^{\circ}C$)	s	solar
T_f	temperature of the ejector working fluid ($^{\circ}C$)		
T_g	temperature of vapor generation ($^{\circ}C$)		
T_r	ejector cycle evaporator temperature ($^{\circ}C$)		

bromide/water absorption chiller can reach 0.7 (Herold et al., 1996), while the COP of an ejector cycle, under the same operation temperatures can reach 0.48 (Pridasawas and Lundqvist, 2007). A low value of the COP implies that a large optimum collector area is needed in order to meet the cycle heat load requirements. Therefore, potential advantages arising from the lower cost of an ejector cooling system are balanced by the requirement of increased collector area.

Solar-assisted ejector systems are usually simulated on an hourly basis (Vidal and Colle, 2004), by using data from typical meteorological year (TMY) databases, which are readily available at meteorological services of developed countries. However, good quality TMY database are seldom available in developing and undeveloped countries, which could take advantage of solar-assisted systems to reduce their expenditures in primary energy sources like fossil fuels. Monthly averages of global and beam solar radiation incident on horizontal surfaces have recently

become available to several countries, thanks to the successful modeling techniques used to estimate incoming solar radiation derived from satellite data (Pereira et al., 2008). Satellite-derived solar radiation can presently be estimated with uncertainty levels around 5%, according to comparisons with land-based monitoring stations.

The solar fraction, defined as the ratio of solar-supplied heat to total thermal load, is dependent on available solar radiation, collector efficiency, collector surface area, and thermal load. The cost of solar-assisted cooling cycles is therefore linked to the solar fraction, which determines the optimal collector area, and the cost of operating an auxiliary heating system. A proper estimation of hourly, daily, monthly mean, and yearly mean solar fraction allows for correct dimensioning of a solar-assisted cooling system, and for an accurate estimation of capital and operation costs during its life cycle. Varying conditions for available solar radiation exist in every geographical location, which difficults the application of standardized solutions. It is

therefore necessary to develop methodologies for determining the solar fraction of solar-assisted cooling cycles, in order to help the optimization process that can lead to the design and deployment of high-performance, low-cost systems.

One of such design methodologies is the $f-\bar{\phi}$ -chart method as proposed in Klein and Beckman, (1979), which is based on monthly average solar radiation data and the utilizability concept. It constitutes a useful tool that can be applied to the design and optimization of solar cooling systems, as well as to analyze the economical feasibility of these systems for given economical scenarios. The methodology has successfully been used for process heat system design, as well as for cooling applications, by analyzing an optimized ejector cooling system and reporting the results of simulation based on hourly data, which compares well to $f-\bar{\phi}$ -chart predictions (Vidal and Colle, 2004).

In what follows, simulation results are reported, which show that the $f-\bar{\phi}$ -chart method can be validated in terms of the monthly and annual solar fractions. The validation is carried out for the city of Florianópolis, Brazil, (located at 27.6 S), for which a TMY database is available, built from a 14 years long solar radiation data series collected in baseline surface radiation network (BSRN) surface stations (Abreu et al., 2000). Partial results of the present paper are reported in Colle et al. (2004, 2007).

It should be pointed out that the $f-\bar{\phi}$ -chart method is considered to be applicable to design heating systems, in cases for which heat is supplied to the load at a temperature above a specified process heat minimum temperature value. The method is therefore expected not to be applicable if the process heat depends on the loading system temperature. In the case of solar-assisted ejector cooling cycles, the process heat depends not only on the condenser temperature, but also on the vapor generator temperature. It will be shown that the $f-\bar{\phi}$ -chart method can be validated for ejector cooling systems, once a minimum temperature value is properly chosen, which must be sufficiently close to the vapor generator temperature. The methodology is restricted to closed cycle systems, with a constant or near constant coefficient of performance, and which are characterized by a minimum operation temperature, above which all solar-supplied heat is used in the process.

2. The ejector solar cooling system

A solar-assisted ejector cooling system is composed of a solar heating system that supplies heat to a vapor generator, which operates as the heat source in an ejector cooling cycle, as shown in Fig. 1.

The working fluid evaporates in the vapor generator at the saturation temperature T_g and provides the primary stream that flow into the ejector nozzle. The primary stream provides the kinetic energy necessary to impel the secondary flow by mixing with it in the ejector. The mixture of both streams circulates to the condenser and loses heat at a temperature T_c . After the condenser, the flow splits

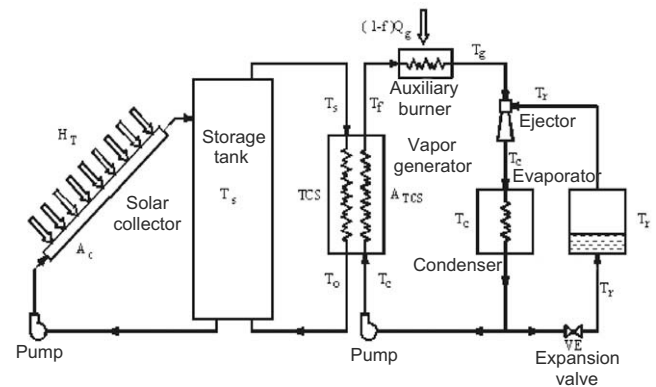


Fig. 1. Solar-assisted ejector cooling system.

into primary, which is pumped back to the vapor generator, and secondary, which flows to the evaporator at T_r after passing through an expansion valve. The ratio of primary to secondary nozzle cross section areas of the ejector is designed in order to achieve the maximum flow ratio in the evaporator, for a given flow ratio of the primary stream. Algorithms for simulation and optimization of the ejector nozzle are reported in Huang et al. (1998, 1999).

An auxiliary heating system is needed if the amount of heat provided by the solar heating system is unable to satisfy the thermal load requirements. The combined operation of solar and auxiliary heating systems guarantees a proper steady state flow rate of refrigerant.

3. Governing equations

A model for the solar-assisted ejector cooling system is developed based on energy conservation principles for three flow circuits: the solar heat collection system, the vapor generation circuit, and the ejector/evaporator circuit.

3.1. Solar heating system

It is composed by the solar collector, the storage tank, and the water side of the vapor generator. A full mixing model is assumed in order to simplify the energy balance of the system: all the fluid inside the storage tank is considered to be at the same temperature, and the system pipes are ideal, without friction and temperature losses.

An energy balance of system leads to the following equation:

$$(mc)_s \frac{dT_s}{dt} = A_c [F_R(\tau\alpha)_n K_{\tau\alpha} G_T - F_R U_L (T_s - T_{ac})] - (UA)_s (T_s - T_{ai}) - \alpha_s Q_s \quad (1)$$

where T_s is the fluid temperature in the storage tank, $(mc)_s$ is the thermal capacity of the heating fluid in the storage tank, $F_R(\tau\alpha)_n$ and $F_R U_L$ are the energy gain and energy loss coefficients of the straight line correlation for a flat plate collector efficiency, A_c is the useful collector area, $(UA)_s$

is the heat loss coefficient of the storage tank T_{ai} and T_{ac} are the ambient temperatures for the storage tank and solar collector, respectively, G_T is the incident solar radiation on the tilted collector surface, $K_{\tau\alpha}$ is the incidence angle modifier of the collector, Q_s is the solar heat supplied by the system to the vapor generator, and α_s is a control flag set to vanish for $T_s \leq T_c$ and set equal to the unity for $T_s > T_c$.

3.2. Vapor generation circuit

The solar heat collection system and the vapor generation circuit are linked through the vapor generator heat exchanger, which receives the solar-supplied heat Q_s . The heating load needed in the vapor generator is Q_g , which is related to the solar-supplied heat by the hourly solar fraction f :

$$F = Q_s / Q_g \quad (2)$$

The hourly solar fraction in the vapor generator varies from 0 (no heat supplied by the solar heat collection system) to 1 (as when $Q_g = Q_s$, the total of the required heat being supplied by solar energy). If the solar-supplied heat is higher than the required load in the vapor generator (a solar fraction higher than 1), then the energy surplus is stored in the reservoir. In cases where the solar fraction is lower than 1, an auxiliary heat source is needed, probably in the form of an electrical heater, or as an oil, gas or biomass burner. Therefore, the amount of auxiliary heat needed by the vapor generation circuit is given by:

$$Q_{aux} = Q_g - Q_s = Q_g(1 - Q_s / Q_g) = (1 - f)Q_g \quad (3)$$

The annual solar fraction f_a is the average of the hourly solar fraction f for all hours in a year.

The temperatures in the vapor circuit shown in Fig. 1 are: the condenser temperature T_c , the temperature after the vapor generator T_f , and the temperature after the auxiliary burner T_g , which is the saturation temperature of the refrigerant at the high-pressure side of the vapor generation circuit.

Depending on the solar fraction, the vapor generator can work either as a single-phase heat exchanger or as a two-phase heat exchanger. This gives origin to two different operation regimes for the heat exchanger.

Case I: Vapor generator acting as a single-phase heat exchanger ($T_f < T_g$)

For low solar fractions, the solar heating system is able to supply only sensible heat to the vapor generator, and the refrigerant does not reach a saturated state. In this case, and according to heat exchanger theory, the heat supplied to the vapor generator is given by:

$$Q_s = W_{min} \varepsilon_s (T_s - T_c) = \omega_{ej} c_{rl} (T_f - T_c) \quad (4)$$

where c_{rl} is the specific heat of the subcooled refrigerant, and ε_s the single-phase heat exchanger effectiveness, defined as

$$\varepsilon_s = \omega_{ej} c_{rl} (T_f - T_c) / W_{min} (T_s - T_c) \quad (5)$$

where ω_{ej} is the mass flow rate of the refrigerant, $W_{min} = \min\{\omega c_p\}_s, \omega_{ej} c_{rl}\}$, where $(\omega c_p)_s$ is the hourly thermal capacitance of the heating fluid. The heat exchanger effectiveness ε_s is a function of $(U_s A_s)$, the product of the global heat transfer coefficient and the surface area of the vapor generator, and of W_{min} . In this single-phase flow situation, the surface area equals the total surface area of the heat exchanger, A_{TCS} . The limit temperature for the heating fluid is achieved when the refrigerant reaches the saturation temperature T_g at the end of the vapor generator, with a vapor quality of $x_f = 0$. It is possible to compute this limit temperature T_{sl} by replacing T_g for T_f in Eq. (5) and solving for $T_s = T_{sl}$, as

$$T_{sl} = T_c + \omega_{ej} c_{rl} (T_g - T_c) / W_{min} \varepsilon_s \quad (6)$$

If the solar fraction is such that the refrigerant temperature does not reach the onset of saturation after flowing through the vapor generator, then the temperature T_f can be solved as function of T_s :

$$T_f = T_c + W_{min} \varepsilon_s (T_s - T_c / \omega_{ej} c_{rl}) \quad (7)$$

Case II: Vapor generator acting as a two-phase heat exchanger ($T_f = T_g$)

For a high enough solar fraction, the solar heat supplied will increase the refrigerant temperature until it reaches a saturated state, and then provide latent heat. In this case part of the heat exchanger area A_{TCS} is occupied by liquid and part is occupied by vapor.

The heat input in this two-phase flow case is a function of the saturated liquid and vapor enthalpies $h_l(T_g)$ and $h_v(T_g)$:

$$Q_s = \omega_{ej} (h_l - h_c + h_{lv} x_f) \quad (8)$$

where $h_{lv} = h_v - h_l$, x_f is the vapor quality, and h_c is the enthalpy of the subcooled liquid at temperature T_c . The maximum value of Q_s is the amount of heat required to change the thermodynamic state of the refrigerant from subcooled liquid at T_c to saturated vapor ($x_f = 1$) at T_g , or $Q_s = Q_g = \omega_{ej} (h_v - h_l)$. The area A_s of the heat exchanger filled with liquid is given by $A_s = A_{TCS} - A_v$, where A_v is the area of the vapor generator where actual phase change takes place. In this case, according to heat exchanger theory (Incropera and De Witt, 2002), the effectiveness values for the single-phase (ε_s) and the two-phase (ε_{ev}) sections of the vapor generator are given by

$$\varepsilon_s \left(\frac{U_s A_s}{W_{min}}, \frac{W_{max}}{W_{min}} \right) = \frac{\omega_{ej} c_{rl} (T_g - T_c)}{W_{min} (T_i - T_c)} \quad (9)$$

and

$$\varepsilon_{ev} = 1 - \exp \left(- \frac{U_{ev} A_{ev}}{(\omega c_p)_s} \right) = \frac{(T_i - T_s)}{(T_g - T_s)} \quad (10)$$

In Eq. (10), $U_{ev} A_{ev}$ is the product of the global heat transfer coefficient and the surface area of the evaporator section of the vapor generator, and T_i is the temperature

of the heating fluid at the transition section of the vapor generator that sets the limit for the single-phase and two-phase regions, as illustrated in Fig. 2.

Eliminating the unknown transition temperature T_i from Eqs. (9) and (10) results in the following expression:

$$T_c + \frac{\omega_{ej}c_{rl}}{\varepsilon_s \dot{W}_{min}}(T_g - T_c) = T_s + \varepsilon_{ev}(T_g - T_s) \quad (11)$$

Then, an energy balance in the evaporator section of the vapor generator yields

$$(\text{LMDT})_{ev} U_{ev} A_{ev} = \omega_{ej}(h_f - h_l) = \omega_{ej} h_{lv} x_f \quad (12)$$

where (LMDT)_e is the logarithmic mean temperature difference in the evaporator section, given by

$$(\text{LMDT})_{ev} = (T_s - T_i) / \ln \left(\frac{T_s - T_g}{T_i - T_g} \right) \quad (13)$$

From Eqs. (12) and (13) it follows that

$$(T_s - T_i) U_{ev} A_{ev} = \omega_{ej} h_{lv} x_f \ln \left(\frac{T_s - T_g}{T_i - T_g} \right) \quad (14)$$

and Eq. (10) can also be written as

$$(T_i - T_s) = (T_g - T_s) \varepsilon_{ev} \quad (15)$$

or, equivalently:

$$\begin{aligned} (T_i - T_g) &= (T_s - T_g) + (T_g - T_s) \varepsilon_{ev} \\ &= (T_s - T_g)(1 - \varepsilon_{ev}) \end{aligned} \quad (16)$$

The temperature differences $T_i - T_g$ given by Eq. (16), and $T_i - T_s$ given by Eq. (15) are replaced into Eq. (14), leading to

$$(T_g - T_s) \varepsilon_{ev} U_{ev} A_{ev} = \omega_{ej} h_{lv} x_f \ln(1 - \varepsilon_{ev}) \quad (17)$$

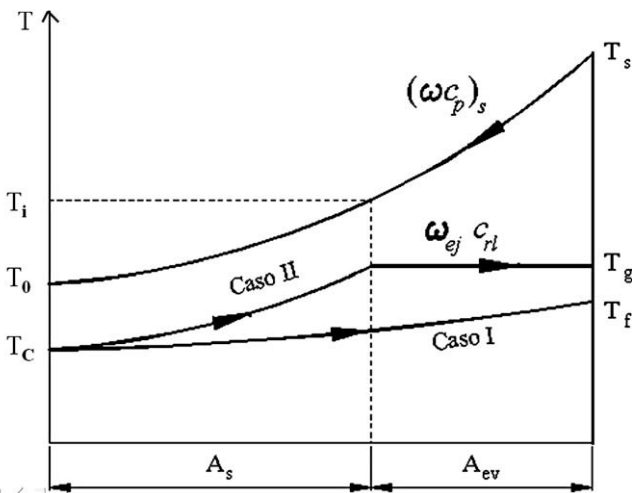


Fig. 2. Temperature paths for heating fluid and refrigerant in the vapor generator.

By subtracting T_g from each side of Eq. (11), and replacing $T_g - T_s$ in the form given by Eq. (17) into the resulting expression, it is possible to obtain

$$\begin{aligned} (T_g - T_c) \left(\frac{\omega_{ej}c_{rl}}{\varepsilon_s \dot{W}_{min}} - 1 \right) U_{ev} A_{ev} \varepsilon_{ev} \\ = \omega_{ej} h_{lv} x_f (\varepsilon_{ev} - 1) \ln(1 - \varepsilon_{ev}) \end{aligned} \quad (18)$$

By replacing the expression of ε_{ev} given by Eq. (10) into Eq. (18), it follows that

$$\begin{aligned} x_f \varepsilon_s \omega_{ej} h_{lv} \exp \left(\frac{-U_{ev} A_{ev}}{(\omega c_p)_s} \right) \\ = (T_g - T_c) (\omega c_p)_s \times \left(\frac{\omega_{ej}c_{rl}}{\dot{W}_{min}} - \varepsilon_s \right) \left[1 - \exp \left(\frac{-U_{ev} A_{ev}}{(\omega c_p)_s} \right) \right] \end{aligned} \quad (19)$$

and the total area of the heat exchanger is given by the sum of the liquid phase area and the two-phase area as:

$$A_s + A_{ev} = A_{TCS} \quad (20)$$

For any given vapor quality x_f at the outlet of the vapor generator, it is possible to compute the unknown areas A_{ev} and A_s by combining Eqs. (19) and (20).

Eqs. (11) and (20) can also be solved in terms of A_{ev} and A_s for known values of T_s .

In the circumstance the vapor quality x_f inside the vapor generator reaches the unity, the solar fraction f also reaches the unity. Therefore there is no need for auxiliary heating, and the evaporator area A_{ev} of the vapor generator reaches a maximum value A_{evmax} , for which case the heating fluid temperature T_s reaches T_{sv} , which from Eq. (11) can be expressed as follows:

$$T_{sv} = \left[T_c + \frac{\omega_{ej}c_{rl}}{\varepsilon_s \dot{W}_{min}}(T_g - T_c) - \varepsilon_{ev} T_g \right] / (1 - \varepsilon_{ev}) \quad (21)$$

The temperature T_{sv} is defined as the temperature of the heating fluid, that results in the refrigerant reaching a saturated vapor state ($x_f = 1$).

The vapor quality can be obtained from an energy balance in the evaporator section, as

$$x_f = \varepsilon_{ev}(T_s - T_g) (\omega c_p)_s / \omega_{ej} h_{lv} \quad (22)$$

Eq. (22) can also be obtained from Eq. (18) by replacing in it the evaporator effectiveness ε_{ev} given by Eq. (10).

3.3. Ejector/evaporator circuit

In this circuit, the ejector is assumed to operate steadily at its optimum efficiency point. The refrigeration load Q_r is related to the heat supply load to the vapor generation circuit by means of the coefficient of performance COP, as

$$Q_g = Q_r / \text{COP} \quad (23)$$

The coefficient of performance of an ejector cooling cycle is known to be a function of the condenser temperature T_c , the vapor generation temperature T_g , and the evaporator temperature T_r .

4. Solar fraction computation

For given values of the heat exchanger area A_{TCS} and the thermal capacitance ratio $(\omega c_p)_s / \omega_{ej} c_{rl}$, T_{sl} can be determined from Eq. (6). For the case of $x_f = 1$, Eq. (19) and Eq. (20) can be solved in terms of A_s and A_{evmax} . T_{sv} is thus obtained from Eq. (21).

The values of T_{sl} for which the phase change regime begins are shown in Fig. 3 as function of heat exchanger area. It is observed that lower values of thermal capacitance ratio result in higher values of T_{sl} needed for the onset of phase change within the heat exchanger.

Fig. 4 shows the values of T_{sv} as function of the heat exchanger area A_{TCS} , for different values of heat capacitance ratio. It can be seen that, similarly to what is observed regarding T_{sl} , higher values of T_{sv} are observed for lower values of the heat capacitance ratio. This indicates that it is desirable to have a combination of low heat capacitance ratio and relatively high heat exchanger area, in order to achieve a saturated vapor state for the refrigerant at the outlet of the vapor generator. It also indicates

that heat exchanger areas larger than 3 m^2 can be considered as very large, therefore having a negligible effect on T_{sv} .

If a phase change process does occur in the refrigerant side, then the evaporator maximum area is dependent on the reservoir thermal capacitance, and on the heat exchanger area, as seen in Fig. 5. The maximum evaporator area appears to be asymptotic with the heating fluid hourly thermal capacitance for fixed values of heat exchanger area.

For given values of $(\omega c_p)_s / \omega_{ej} c_{rl}$ and A_{TCS} , Eqs. (11), (20), and (22) can be solved in terms of x_f , A_s and A_{ev} , for each specified value of T_s . The hourly fraction f is thus evaluated from Eqs. (8) and (2), once the cooling capacity and COP are specified.

Figs. 6–8 display the hourly solar fraction behavior as a function of the heating fluid temperature, for different thermal capacitance ratios $(\omega c_p)_s / \omega_{ej} c_{rl}$, and for constant heat exchanger areas of 0.2 m^2 , 2 m^2 and 3 m^2 . It can be seen that the solar fraction value increases for increasing heat exchanger area, with an asymptotic limit reached for relatively high values of A_{TCS} .

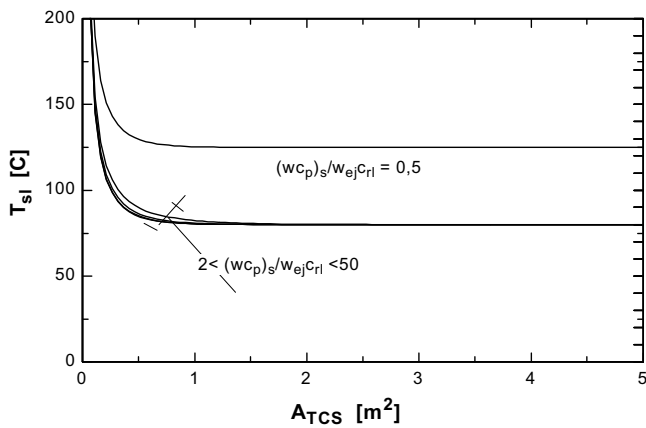


Fig. 3. Temperature T_{sl} at the beginning of phase change phenomena as a function of A_{TCS} for constant values of thermal capacitance ratio.

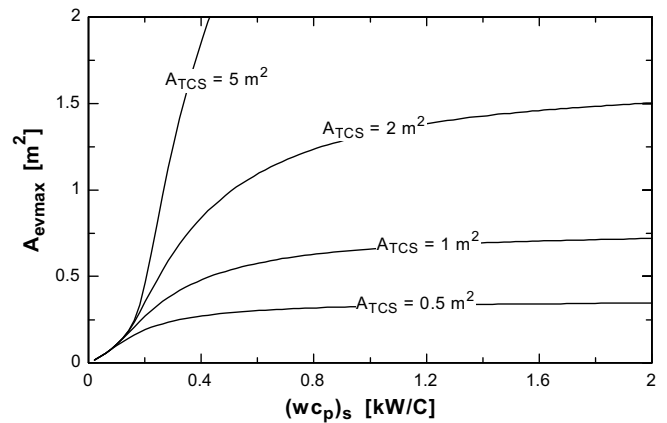


Fig. 5. Maximum two-phase heat exchanger area A_{evmax} as a function of storage thermal capacity for constant values of A_{TCS} .

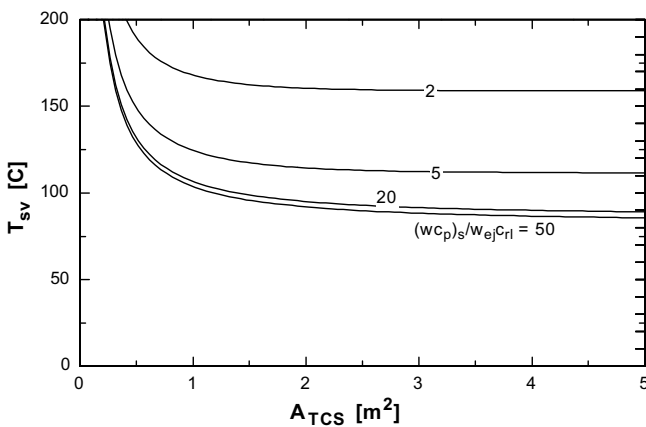


Fig. 4. Temperature T_{sv} at the beginning of phase change phenomena as a function of A_{TCS} for constant values of thermal capacitance ratio.

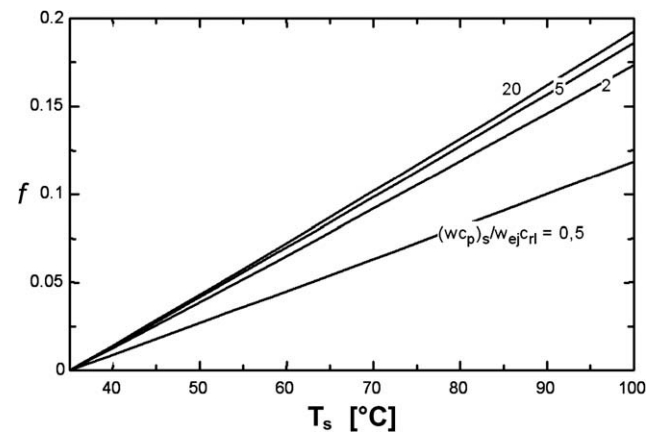


Fig. 6. Hourly solar fraction computed as a function of T_s for constant values of thermal capacitance and $A_{TCS} = 0.2 \text{ m}^2$.

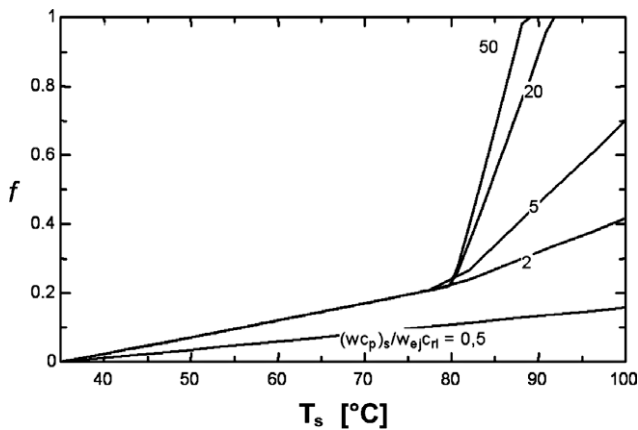


Fig. 7. Hourly solar fraction computed as a function of T_s for constant values of thermal capacitance and $A_{TCS} = 2 \text{ m}^2$.

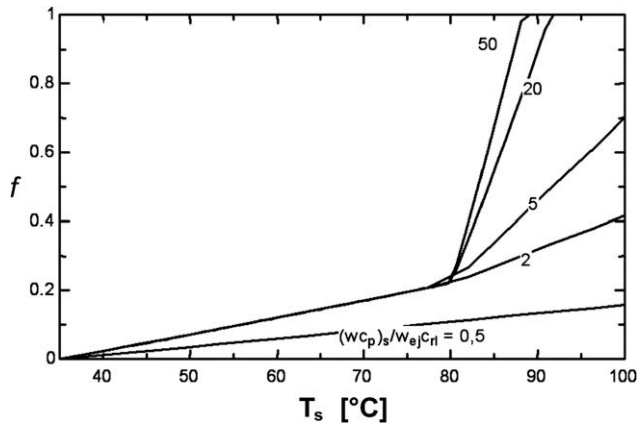


Fig. 8. Hourly solar fraction computed as a function of T_s for constant values of thermal capacitance and $A_{TCS} = 3 \text{ m}^2$.

For constant heat exchanger areas, the solar fraction increases with an increase on the thermal capacitance ratio. For relatively low values of heat exchanger area, the solar fraction is proportional to temperature. This behavior is expected, since a low temperature heat exchange results in one-phase, sensible heat being transferred to the refrigerant circuit.

For relatively high values of heat exchanger area, the refrigerant temperature reaches a saturated state, and phase change occurs, which in turn results in higher values of solar fraction.

The sudden slope change on Fig. 7 and Fig. 8 at $T_s = T_{s1}$ is related to the transition from one-phase to two-phase flow in the heat exchanger, transition which is more notorious at higher heat exchanger areas.

For given refrigeration load Q_r and COP, the vapor reservoir heating requirement Q_g can be computed from Eq. (23). For case I, because of Eq. (4), Eq. (1) becomes a linear differential equation that can be solved in a straightforward manner. Then, the solar-supplied heat can be computed

from Eq. (4), and then the solar fraction is directly computed from Eq. (2).

For case II, the solution procedure is more complex. Eq. (1) is simultaneously solved with Eqs. (8), (11), (20), and (22), in order to find T_s , x_f , A_{ev} and A_s . In cases when T_s becomes greater than T_{sv} , the storage capacity $(\omega c_p)_s$ should be controlled in order to maintain a constant value of T_g . For $T_s > T_{sv}$, Eq. (11) is used to determine $(\omega c_p)_s$ for each value of T_s obtained from Eq. (1), by considering the input heat rate equal to its maximum value given by

$$Q_s = Q_g = \omega_{ej}(h_v - h_c) \quad (24)$$

In this case the evaporator area A_{ev} remains equal to its maximum value A_{evmax} , and therefore, it is possible to find the minimum value of A_s from Eq. (20), as $A_{s \text{ min}} = A_{TCS} - A_{evmax}$.

Once Q_s is thus determined, then the solar fraction f can be computed from Eq. (2) and Eq. (3) is used to find the required value of auxiliary heating.

Results are presented in the following section for the parameters which determine an optimal solar-assisted cooling system, as in (Vidal and Colle, 2004) and (Colle, 2004).

5. Simulation results

The parameters used in the simulations are those for an optimized ejector cooling cycle:

$$Q_r = 10.55 \text{ kW (3 tons of refrigeration)}$$

$$T = 80^\circ\text{C}, T_c = 35^\circ\text{C}, T_r = 8^\circ\text{C}, T_{ac} = 25^\circ\text{C}, T_{ai} = 30^\circ\text{C}$$

$$F_R(\tau\alpha)_n = 0.78, \text{ and } F_R U_L = 0.003 \text{ kW/m}^2\text{K}$$

Simulations are performed for a COP of 0.6 using R142b as the working fluid. The COP 0.6 corresponds to the case of a cascading cooling ejector cycle assisted by a mechanical booster as analyzed in (Arbel and Sokolov, 2004). The storage tank thermal capacity $(m c_p)_s$ is variable,

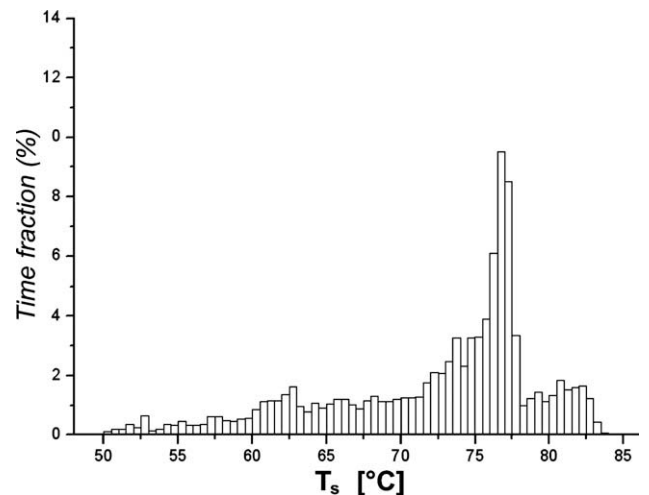


Fig. 9. Occurrences of T_s with time for $A_c = 30 \text{ m}^2$.

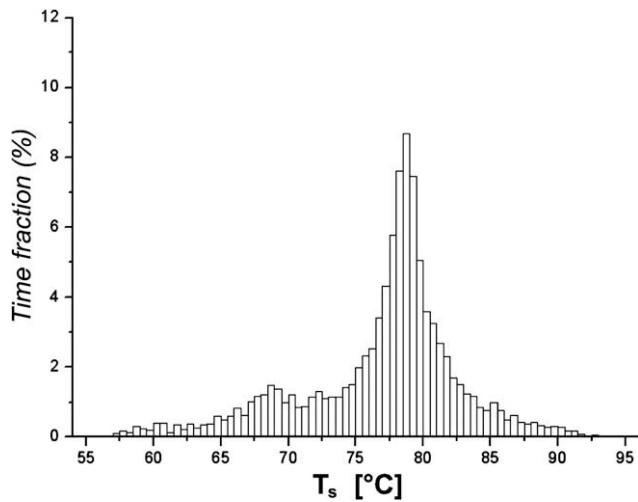


Fig. 10. Occurrences of T_s with time for $A_c = 50 \text{ m}^2$.

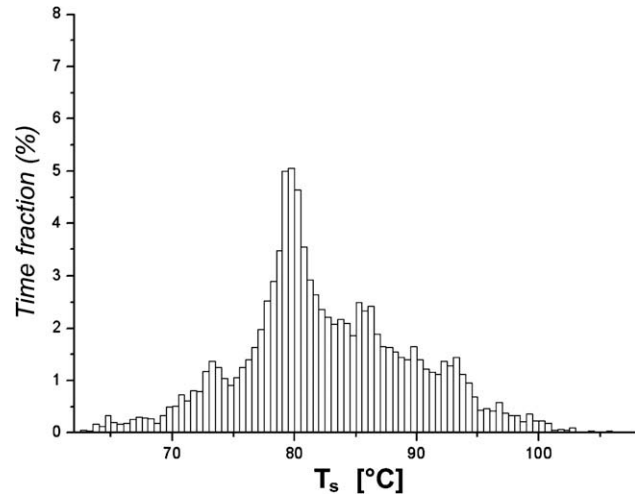


Fig. 11. Occurrences of T_s with time for $A_c = 80 \text{ m}^2$.

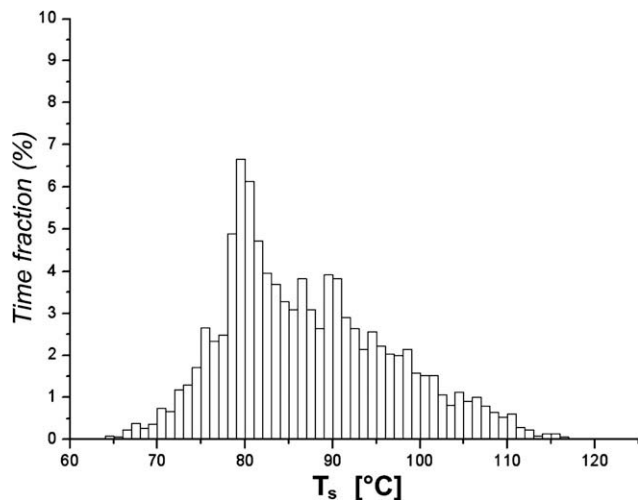


Fig. 12. Occurrences of T_s with time for $A_c = 100 \text{ m}^2$.

defined as the value that is necessary in order to have 75 kg of heating water per square meter of collector area A_c . For the present numerical example, the global heat transfer coefficients are $U_s = 2 \text{ kW/m}^2\text{K}$, and $U_{ev} = 1 \text{ kW/m}^2\text{K}$.

Figs. 9–12 display the frequency distribution of the reservoir temperature T_s occurrences for different collector areas from 30 to 100 m^2 , for a fixed heat capacitance ratio of 50.

It can be observed that as the collector area increases, the most frequent temperature approaches $80 \text{ }^\circ\text{C}$, a critical value of temperature very close to the chosen value of $T_g = 80 \text{ }^\circ\text{C}$. This behavior is expected, since the phase change process starts at temperature values higher than T_g , during which the heat transfer to the vapor generator depends on T_g and the vapor quality x_f in the refrigerant fluid.

The occurrences of hourly solar fractions for collector areas $A_c = 100$ and 150 m^2 are shown in Figs. 13 and Fig. 14, respectively. The heat capacitance ratio in both

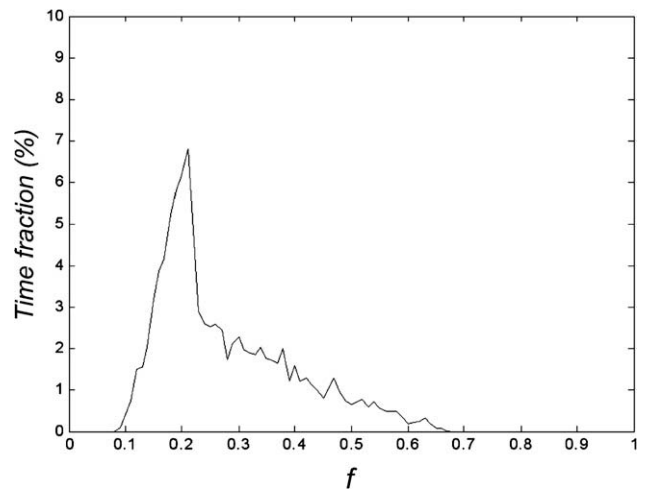


Fig. 13. Occurrences of the solar hourly fraction f for $A_c = 100 \text{ m}^2$.

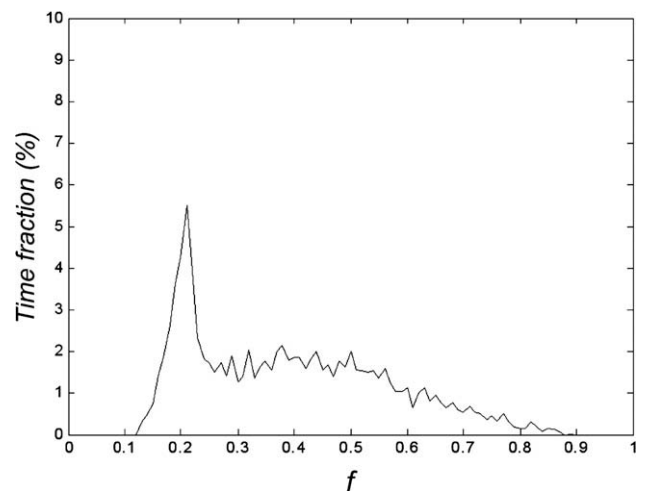


Fig. 14. Occurrences of the hourly solar fraction f for $A_c = 150 \text{ m}^2$.

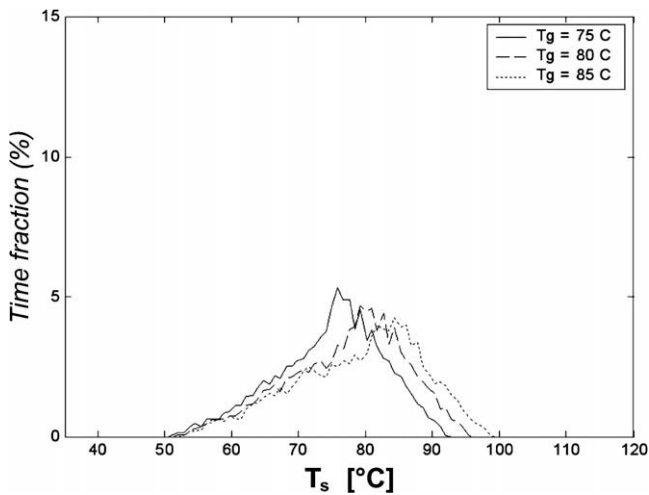


Fig. 15. Occurrences of T_s for three different vapor generator temperatures, with collector area $A_c = 100 \text{ m}^2$ and heat capacitance ratio of 5.

cases is 5. It can be observed that increased collector area results in an enhancement on the occurrence distribution of higher values of hourly solar fraction. The peak around the solar fraction equal to 0.2 can be explained by the shape of f in Fig. 8, for lower thermal capacitance ratio, in which case, the frequency of heating fluid temperatures higher than $80 \text{ }^\circ\text{C}$ is low.

The frequency distribution of T_s for $A_c = 100 \text{ m}^2$ is shown in Fig. 15 as a function of three different vapor generator temperatures: 75, 80 and $85 \text{ }^\circ\text{C}$, with a heat capacitance ratio of 5.

From a statistical point of view, it can be argued that the mean value for T_s is in each case slightly lower than T_g , which seems to indicate that the minimum temperature needed for applying the utilizability concept could be lower than the vapor generation temperature.

6. Comparison with $f-\bar{\phi}$ -chart method

The annual solar fraction f_a associated with the ejector cycle is a function of A_c , T_c , T_g , A_{TCS} , $\omega_{ej}c_{rl}$ and $(\omega c_p)_s$. On the other hand, the annual solar fraction $f_{\bar{\phi}}$ from the $f-\bar{\phi}$ -chart method is a function of A_c , T_{min} and εW_{min} . Both f_a and $f_{\bar{\phi}}$ increase with increased heat exchanger area and with increased heat capacitance. For a given value of T_{min} , the fraction $f_{\bar{\phi}}$ increases with εW_{min} , reaching an asymptotic value for infinite εW_{min} . As the heat exchanger area A_{TCS} decreases, T_{sv} increases while f_a decreases. This suggests that if $T_{min} = T_g$, a decrease on A_{TCS} implies a decrease of both f_a and $f_{\bar{\phi}}$.

These tendencies are valid for fixed values of W_{min} and $(\omega c_p)_s$. The present work is not intended to determine a correlation between εW_{min} , $\omega_{ej}c_{rl}$, $(\omega c_p)_s$ and A_{TCS} . Instead of doing this, the paper is intended to show that the $f_{\bar{\phi}}$ correlation can be used to estimate the annual solar fraction, once a properly minimum temperature T_{min} is chosen. Therefore only the case of very large heat exchanger area is analyzed.

6.1. Annual solar fraction computed from hourly data

Fig. 16 shows the mean annual solar fraction behavior as function of collector area for different values of heat exchanger area. It is seen that the solar fraction increases with collector area. A COP of 0.2476 is used for a single stage system operating with R141b. The heat exchanger area of 5 m^2 can be considered as a relatively large value, above of which there will only be a marginal increase on the solar fraction.

Fig. 17 shows the mean annual solar fraction behavior as a function of the product of coefficient of performance and collector area. The figure demonstrates that it is possible to represent the solar fraction in a single graph for different values of COP. In other words, it is possible to represent the solar fraction through a group of variables, thus allowing independence from the COP parameter. This

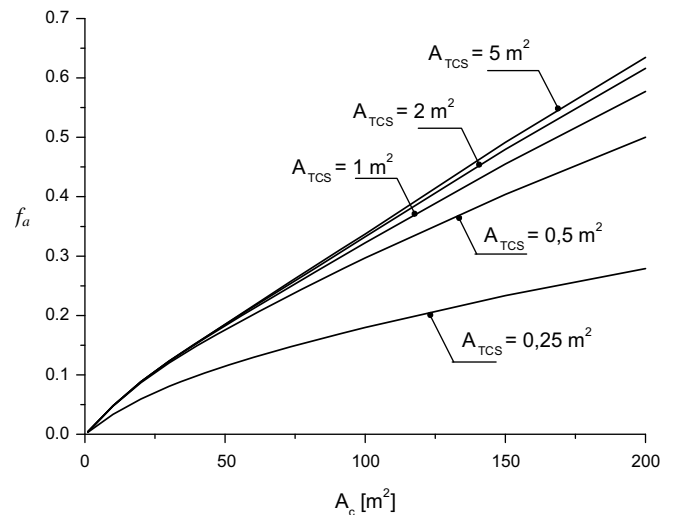


Fig. 16. Mean annual solar fraction as function of collector and heat exchanger area.

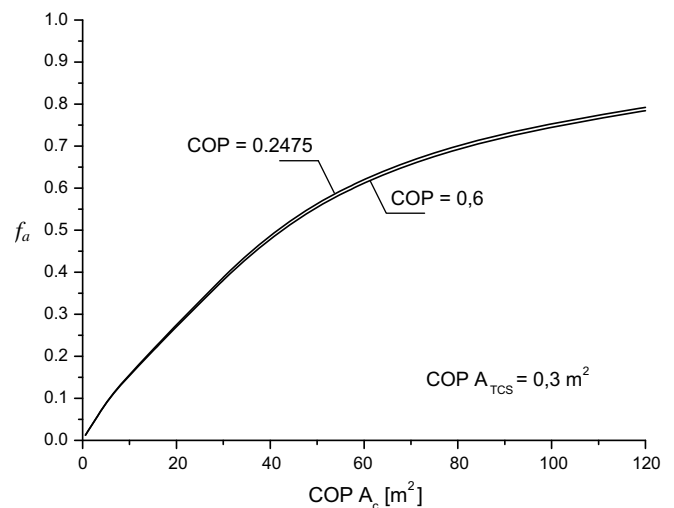


Fig. 17. Mean annual solar fraction as function of the $\text{COP} \times A_c$ product.

result is interesting for validating the $f-\bar{\phi}$ -chart correlation against the simulation results, because according to Klein and Beckman, (1979), $f_{\bar{\phi}}$ among other parameters is a function of A_c/Q_g , and thus from Eq. (23) it is also a function of COP A_c/Q_g .

6.2. Adjustment of the $f-\bar{\phi}$ -chart correlation

The numerical results from the hourly simulations here presented have been used to adjust the solar fraction correlation presented in Klein and Beckman, (1979). Here, W_{\min} is the hourly thermal capacitance of the refrigerant fluid. Different minimum temperatures were tested; above of which all the heat is useful to the system, in agreement with the basic definitions of the $f-\bar{\phi}$ -chart method. A numerical value of εW_{\min} is determined for each of the specified values of T_{\min} and A_{TCS} , in order to minimize the error between simulated solar fraction and that from the $f-\bar{\phi}$ -chart method.

The mean annual solar fraction computed with the $f-\bar{\phi}$ -chart method is shown in Fig. 18 as a function of εW_{\min} for different values of collector area. It is observed that increased values of εW_{\min} result in an increasing solar fraction, which exhibits an asymptotic behavior more pronounced as the collector area is decreased. The tendency is expected, since relatively large heat exchanger areas and W_{\min} values increase the ability of the system to transfer heat. Furthermore, it is found that values of εW_{\min} around 100,000 are equivalent to a heat exchanger of infinite area, for all collector area values.

A direct comparison for the mean annual solar fraction between the simulation results and the $f-\bar{\phi}$ -chart method is depicted in Fig. 19, for the case in which $T_{\min} = T_g = 80^\circ\text{C}$. Table 1 shows the numerical data for solar fraction and percentage error as function of collector area for this case. The error $\delta^2 \times 10,000$ is the sum of the squared relative errors given in the fourth column of Table 1.

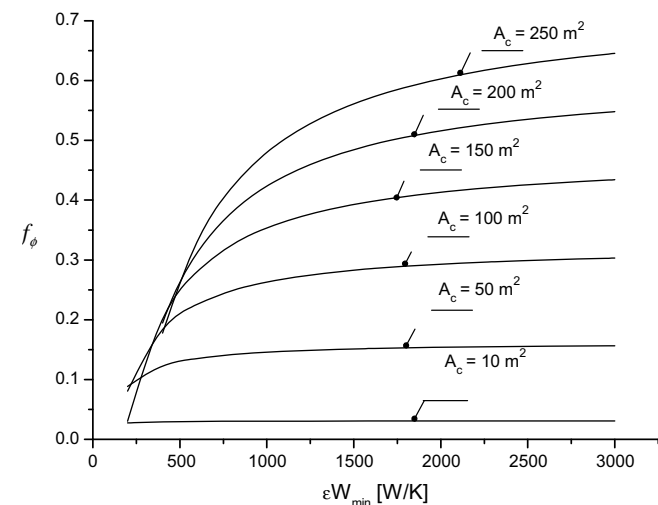


Fig. 18. Mean annual solar fraction $f_{\bar{\phi}}$ as a function of εW_{\min} and collector area A_c .

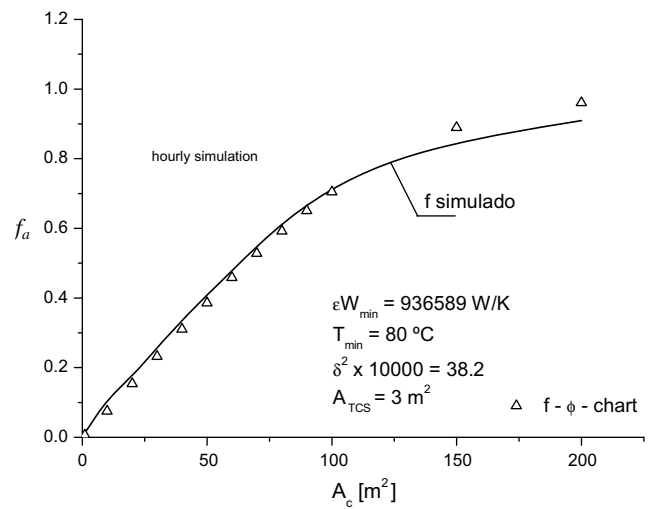


Fig. 19. Comparison between simulation and $f-\bar{\phi}$ -chart results for mean annual solar fraction as a function of collector area A_c , for $T_{\min} = 80^\circ\text{C}$.

Table 1
Numerical results corresponding to Fig. 19

A_c (m ²)	$f_{\text{simulated}}$	$f-\bar{\phi}$ -chart	Error $\left \frac{f_{\bar{\phi}} - f_{\text{simulated}}}{f_{\text{simulated}}} \right \times 100\%$
10	0.1029	0.07492	27.19145
20	0.1783	0.1534	13.96523
30	0.257	0.2319	9.76654
40	0.3352	0.31	7.5179
50	0.4088	0.3855	5.69961
60	0.4788	0.4587	4.19799
70	0.5471	0.5281	3.47286
80	0.6113	0.592	3.15721
90	0.6654	0.6508	2.19417
100	0.7111	0.7046	0.91408
150	0.8437	0.8891	5.38106

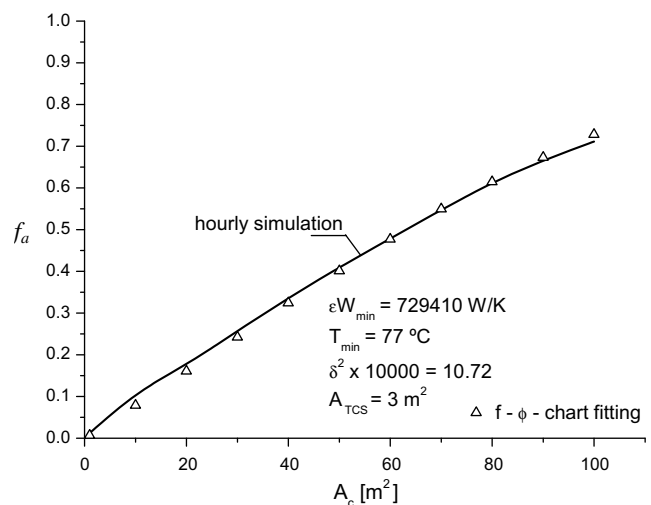


Fig. 20. Comparison between simulation and $f-\bar{\phi}$ -chart results for mean annual solar fraction as a function of collector area A_c , for $T_{\min} = 77^\circ\text{C}$.

Table 2
Numerical results corresponding to Fig. 20

A_c (m ²)	$f_{\text{simulated}}$	$f_{\text{f-}\bar{\phi}\text{-chart}}$	Error $\left \frac{f_{\bar{\phi}} - f_{\text{simulated}}}{f_{\text{simulated}}} \right \times 100\%$
10	0.1029	0.07881	23.4110
20	0.1783	0.1606	9.92709
30	0.257	0.2424	5.68093
40	0.3352	0.3239	3.37112
50	0.4088	0.4013	1.83464
60	0.4788	0.4771	0.35505
70	0.5471	0.5496	0.45695
80	0.6113	0.6146	0.53983
90	0.6654	0.6728	1.11211
100	0.7111	0.728	2.3766
150	0.8437	0.9178	8.78274

It can be observed that good agreement exists between both methodologies, with error levels decreasing as collector area approaches a value of 100 m².

The comparison for the mean annual solar fraction between the simulation results and the $f_{\text{f-}\bar{\phi}\text{-chart}}$ method for the case in which $T_{\text{min}} = 77$ °C is depicted in Fig. 20. Table 2 shows the numerical data for solar fraction and percentage error as function of collector area for this case. It is seen that good agreement exist between both methodologies, and that the best fit occurs for collector areas of 70 and 80 m², which is in agreement to the optimum collector area of 80 m² determined by Vidal and Colle (2004). It is interesting to note that, for Fig. 20, T_{min} is lower than T_g . This result seems to indicate that a lower value of T_{min} also results in good agreement with the $f_{\text{f-}\bar{\phi}\text{-chart}}$ method.

7. Conclusions

A comparison of the solar fraction computation by the $f_{\text{f-}\bar{\phi}\text{-chart}}$ method and by hourly simulation results of a solar-assisted ejector cooling cycle has been carried out, for a particular vapor generator temperature of 80 °C. The simulation is based on energy conservation for three flow circuits: a solar heating circuit, a vapor generation circuit, and an ejector/evaporator circuit. All three circuits are linked by proper energy conservation expressions, and the methodology is able to successfully simulate a wide range of solar fractions, including single-phase and two-phase flow in the vapor generator.

The numerical results show that the simulation results are in good agreement with the $f_{\text{f-}\bar{\phi}\text{-chart}}$ prediction for the annual solar fraction, and that a minimum equivalent utilizability temperature of 77 °C, which is lower than the vapor generation temperature, can be used. The best fit is found for collector areas close to what has been determined in the literature to be an optimum value, for particular load conditions.

The analysis indicates that the simulations presented are a valid design methodology, comparable to the more estab-

lished $f_{\text{f-}\bar{\phi}\text{-chart}}$ method, and that monthly mean radiation data can be used with an acceptable error level for design and analysis purposes in cases when a TMY database is not available.

The methodology is independent of the refrigeration cycle COP, and thus can be used for different combinations of components and refrigeration loads.

The present analysis should be made for other values of the vapor generator temperature. It should also be extended to other refrigerant fluids, in order to find a correlation between vapor generation temperature and the respective equivalent minimum temperatures for the $f_{\text{f-}\bar{\phi}\text{-chart}}$ correlation.

Acknowledgments

The authors acknowledge financial support from CNPq, the National Research Council of Brazil, and PETROBRAS, under contract CT-Petro/FINEP No. 21.01.0387.00, and from the Dirección de Asuntos Internacionales of Pontificia Universidad Católica de Chile.

References

- Abreu, S.L., Colle, S., Almeida, A., Mantelli, S., 2000. Quality control of solar radiation data collected at BSRN – Baseline Surface Radiation Network (<http://bsrn.ethz.ch>) of Florianopolis (in Portuguese). In: Proceedings of the ENCIT 2000 – 8th Brazilian Congress of Thermal Engineering and Sciences, Porto Alegre, October.
- Arbel, A., Sokolov, M., 2004. Revisiting solar-powered ejector air conditioner – the greener the better. *J. Sol. Energ.* 77, 57–66.
- Colle, S., Vidal G.H., Pereira, G.S., 2004. Limites de validade do método de projeto $f_{\text{f-}\bar{\phi}}$ chart para ciclos de refrigeração de ejector assistido por energia solar. In: Proceedings of XII Congresso Ibérico y VII Iberoamericano de Energía Solar, Vigo, Spain, pp. 573–578.
- Colle, S. 2004. Final report of project SIRE SOL, Contract CT-Petro/FINEP No. 21.01.0387.00, Department of Mechanical Engineering/UFSC, November.
- Colle, S., Pereira, G.S., Vidal G.H., 2007. On the validity of a design method to estimate the solar fraction for an ejector cooling system. In: Proceedings of the ISES Solar World Congress, Beijing, pp. 848–852.
- Herold, K., Radermacher, R., Klein, S., 1996. Absorption Chillers and Heat Pumps. CRC Press.
- Huang, B.J., Chang, J.M., Petrenko, V.A., Zhuk, K.B., 1998. Solar ejector cooling system using refrigerant R141b. *J. Sol. Energ.* 64, 223–226.
- Huang, B.J., Chang, J.M., Petrenko, V.A., 1999. A 1-D analysis of ejector performance. *Int. J. Refrig.* 22, 354–364.
- Incropera, F.P., De Witt, D.P., 2002. Introduction to Heat Transfer, fourth ed. John Wiley & Sons.
- Klein, S.A., Beckman, W.A., 1979. A general design method for closed-loop solar energy systems. *J. Sol. Energ.* 22, 269–282.
- Pereira, E., Martins, F., Silva, S., Abreu, S., Colle, S., 2008. Solar energy scenarios in Brazil, Part I: Resource assessment. *Energy Policy* 36, 2843–2854.
- Pridasawas, W., Lundqvist, P., 2007. A year-round dynamic simulation of a solar-driven ejector refrigeration system with iso-butane as a refrigerant. *Int. J. Refrig.* 30 (5), 840–850.
- Vidal, G.H., Colle, S., 2004. Modeling and hourly simulation of a solar ejector cooling system. *J. Appl. Therm. Eng.* 26, 663–672.